

This discussion paper is/has been under review for the journal *Atmospheric Chemistry and Physics (ACP)*. Please refer to the corresponding final paper in *ACP* if available.

**Observations and  
analysis using the  
extended CMAM**

S. R. Beagley et al.

# First multi-year occultation observations of CO<sub>2</sub> in the MLT by ACE satellite: observations and analysis using the extended CMAM

S. R. Beagley<sup>1</sup>, C. D. Boone<sup>2</sup>, V. I. Fomichev<sup>1</sup>, J. J. Jin<sup>1</sup>, K. Semeniuk<sup>1</sup>,  
J. C. McConnell<sup>1</sup>, and P. F. Bernath<sup>2,3</sup>

<sup>1</sup>Department of Earth and Space Science and Engineering, York University,  
Toronto, Ontario, Canada

<sup>2</sup>Department of Chemistry, University of Waterloo, Waterloo, Ontario, Canada

<sup>3</sup>Department of Chemistry, University of York, Heslington, York, UK

Received: 6 March 2009 – Accepted: 18 April 2009 – Published: 11 May 2009

Correspondence to: S. R. Beagley (beagley@nimbus.yorku.ca)

Published by Copernicus Publications on behalf of the European Geosciences Union.

Title Page

Abstract

Introduction

Conclusions

References

Tables

Figures

◀

▶

◀

▶

Back

Close

Full Screen / Esc

Printer-friendly Version

Interactive Discussion



## Abstract

This paper presents the first multi-year global set of observations of CO<sub>2</sub> in the mesosphere and lower thermosphere (MLT) obtained by the ACE-FTS instrument on SCISAT-I, a small Canadian satellite launched in 2003. The observations use the solar occultation technique and document the fall-off in the mixing ratio of CO<sub>2</sub> in the MLT region. The beginning of the fall-off of the CO<sub>2</sub>, or “knee” occurs at about 78 km and lies higher than in the CRISTA measurements (~70 km) but lower than in the SABER 1.06 (~82 km) and much lower than in rocket measurements. We also present the measurements of CO obtained concurrently which provide important constraints for analysis. We have compared the ACE measurements with simulations of the CO<sub>2</sub> and CO distributions in the vertically extended version of the Canadian Middle Atmosphere Model (CMAM). Applying standard chemistry we find that we cannot get agreement between the model and ACE CO<sub>2</sub> observations although the CO observations are adequately reproduced. There appears to be about a 10 km offset compared to the observed ACE CO<sub>2</sub>, with the model knee occurring too high. In analysing the disagreement, we have investigated the variation of several parameters of interest, photolysis rates, formation rate for CO<sub>2</sub>, and the impact of uncertainty in eddy diffusion, in order to explore parameter space for this problem. Our conclusions are that there must be a loss process for CO<sub>2</sub>, about 2–4 times faster than photolysis that will sequester the carbon in some form other than CO and we have speculated on the role of meteoritic dust as a possible candidate. In addition, from this study we have highlighted a possible important role for vertical eddy diffusion in 3-D models in determining the distribution of candidate species in the mesosphere which requires further study.

## 1 Introduction

Carbon dioxide plays an important role in the energetics of the mesosphere and lower thermosphere (MLT) providing the major radiative cooling of the region; however its

ACPD

9, 11551–11587, 2009

## Observations and analysis using the extended CMAM

S. R. Beagley et al.

Title Page

Abstract

Introduction

Conclusions

References

Tables

Figures

◀

▶

◀

▶

Back

Close

Full Screen / Esc

Printer-friendly Version

Interactive Discussion



**Observations and  
analysis using the  
extended CMAM**

S. R. Beagley et al.

abundance in the MLT is still uncertain. It is generally considered to be well-mixed up to at least 70 km but starts to fall off at higher altitudes due to diffusive separation and photolysis. The first CO<sub>2</sub> measurements in the upper atmosphere were in-situ measurements obtained by rocket-borne mass spectrometers (Offermann and Grossmann, 1973; Philbrick et al., 1973; Trinks and Fricke, 1978; Offermann et al., 1981). Emission of the CO<sub>2</sub>v<sub>3</sub> band (asymmetric stretch mode) at 4.3 μm has also been obtained from rocket measurements (e.g., Nebel et al., 1994) and from satellite by the Stratospheric and Mesospheric Sounder (SAMS) (López-Puertas and Taylor, 1989) and Improved Stratospheric and Mesospheric Sounder (ISAMS) experiments (López-Puertas et al., 1998; Zaragoza et al., 2000) up to ~120 km.

Global measurements of CO<sub>2</sub> have been obtained by the Cryogenic Infrared Spectrometers and Telescopes for the Atmosphere (CRISTA) experiment which was flown on two Space Shuttle missions in November 1994 and August 1997. CRISTA measured CO<sub>2</sub> 4.3 μm infrared emission and a non-local thermodynamic equilibrium (non-LTE) model was used to invert the radiances to CO<sub>2</sub> number densities in the 60–130 km range (Kaufmann et al., 2002). They found that the CO<sub>2</sub> volume mixing ratio (VMR) deviated from a well mixed state, which we will call the “knee”, around 70 km. This initial deviation is significantly lower in altitude than the result indicated by the rocket-borne mass spectrometer data mentioned above. They also found significant longitudinal and latitudinal structures in the CO<sub>2</sub> density data.

More recently the Sounding of the Atmosphere using Broadband Radiometry (SABER) experiment which uses broadband radiometry to measure 4.3 μm emission in the MLT region on the Thermosphere-ionosphere-Energetics and Dynamics (TIMED) satellite (e.g. Mertens et al., 2009) has provided *daytime* CO<sub>2</sub> profiles using their version 1.06 (V1.06) retrieval method. For V1.06 retrievals their high latitude results are often compromised by the presence of NO<sup>+</sup> 4.3 μm emission due to electron precipitation in the auroral region. The SABER team have started to address this for V1.07 temperatures (c.f. Mertens et al., 2008; Remsberg et al., 2008) but CO<sub>2</sub> profiles necessary for temperatures are taken from model data.

[Title Page](#)[Abstract](#)[Introduction](#)[Conclusions](#)[References](#)[Tables](#)[Figures](#)[◀](#)[▶](#)[◀](#)[▶](#)[Back](#)[Close](#)[Full Screen / Esc](#)[Printer-friendly Version](#)[Interactive Discussion](#)

**Observations and  
analysis using the  
extended CMAM**

S. R. Beagley et al.

The drawback of using emission measurements of the  $\nu_3$  band at  $4.3 \mu\text{m}$  is that this approach does not give direct information on the  $\text{CO}_2$  abundance, but rather on the population of the vibrationally excited  $\nu_3$  level. On the other hand, the mesosphere is a region where the breakdown of local thermodynamic equilibrium (LTE) conditions starts to occur. The latter means that in order to obtain the  $\text{CO}_2$  abundance from emission measurements, non-LTE models must be used to interpret and invert the data. The population of the vibrationally excited  $\nu_3$  level depends on the emission from this level, the absorption of near-infrared radiation emanating from the sun and from the lower atmosphere, and on collisional excitation and de-excitation by the background species, in particular by excited atomic oxygen,  $\text{O}(^1\text{D})$ . There is also some evidence that highly vibrationally excited hydroxyl molecules affect the  $\text{CO}_2$  asymmetric stretch mode (Kumer et al., 1978). As stated by Kaufman et al. (2002) the  $\text{O}(^1\text{D})$  excitation mechanism and the non-LTE model parameters constitute the most important uncertainties of retrieved  $\text{CO}_2$ . And, as noted above (Mertens et al., 2008; Remsberg et al., 2008) with broadband instruments there is the possibility of contamination from  $\text{NO}^+$   $4.3 \mu\text{m}$  emission from aurora and the ionosphere.

As mentioned above, emission instruments do not directly measure the ground state of  $\text{CO}_2$ . However, for solar occultation measurements the absorption only depends on the  $\text{CO}_2$  density, the kinetic temperature and the pressure and not on the vibrational excitation of the  $\text{CO}_2$  molecules. The drawback, as compared to an emission experiment such as CRISTA is the number of profiles obtained per day. For typical low earth orbit satellites there are  $\sim 30$  profiles (sunrise and sunset) per day. Solar occultation measurements of carbon dioxide have been performed on board Spacelab 1 with the grille spectrometer (Girard et al., 1988) and on Spacelab 3 by the Atmospheric Trace Molecule Spectroscopy (ATMOS) instrument (Rinsland et al., 1992) and in the Atmospheric Laboratory for Applications and Science (ATLAS) 1, 2 and 3 missions (Kaye and Miller, 1996).

The accuracy of  $\text{CO}_2$  measured by the grille spectrometer on Spacelab 1 was limited by the fact that they could not determine pressure and temperature profiles from

[Title Page](#)[Abstract](#)[Introduction](#)[Conclusions](#)[References](#)[Tables](#)[Figures](#)[◀](#)[▶](#)[◀](#)[▶](#)[Back](#)[Close](#)[Full Screen / Esc](#)[Printer-friendly Version](#)[Interactive Discussion](#)

their own measurements. They employed a modified version of the US Standard atmosphere as inputs to their retrievals (Girard et al., 1988), and (potentially significant) errors in these assumed pressure and temperature profiles would lead to errors in the retrieved CO<sub>2</sub> VMR profile.

5 The ATMOS instrument had the benefit of determining pressure and temperature from its own measurements, just as ACE-FTS does. However, the signal-to-noise ratio (SNR) for all but one of the occultations employed in the Spacelab 3 study (Rinsland et al., 1992) was about 74:1, much lower than that achieved by the ACE-FTS (about 350:1) in the spectral region of the strong CO<sub>2</sub> lines. The SNR for the other occultation  
10 used in the ATMOS study was close to 200:1. There were few occultations measured during the Spacelab 3 mission, yielding minimal opportunity for reducing random noise on the profiles through averaging.

## 2 ACE observations

15 The MLT CO<sub>2</sub> observations were obtained using the ACE-FTS, a Fourier Transform Spectrometer, on the Canadian Atmospheric Chemistry Experiment (ACE) satellite SCISAT-1 (Bernath et al., 2005). The ACE-FTS measures temperature and about thirty species involved in stratospheric ozone-related chemistry, tropospheric air quality as well as isotopologues of some of the molecules. ACE-FTS obtains solar occultations from 2.3 μm to 13.3 μm (750–4400 cm<sup>-1</sup>) with a high spectral resolution (0.02 cm<sup>-1</sup>).  
20 The vertical resolution is ~3–4 km. The standard retrieval approach for temperature, pressure, and VMRs are described by Boone et al. (2005).

Using software developed for the next processing version of the ACE-FTS (version 3.0), pressure/temperature (P/T) retrievals were performed for all occultations from February 2004 through August 2007, followed by CO<sub>2</sub> VMR retrievals over the altitude  
25 range 50 to 120 km (~1.0–2.10<sup>-5</sup> hPa) for the same set of occultations. These CO<sub>2</sub> data are used for our analysis. Note that although a CO<sub>2</sub> VMR profile is generated during a P/T retrieval (Boone et al., 2005), this retrieval employs an empirical function and

---

### Observations and analysis using the extended CMAM

S. R. Beagley et al.

---

Title Page

Abstract

Introduction

Conclusions

References

Tables

Figures

◀

▶

◀

▶

Back

Close

Full Screen / Esc

Printer-friendly Version

Interactive Discussion



is perhaps excessively smoothed to be used for data analysis. However, differences between the retrieved CO<sub>2</sub> VMR profile and the CO<sub>2</sub> VMR profile generated during the P/T retrieval are used in the calculation of error estimates.

Both the P/T and VMR retrieval approaches employ the analysis of microwindows, small (typically ~0.4 cm<sup>-1</sup> wide) regions of the spectrum with minimal interference from other molecules. The same microwindow set was used for both pressure/temperature retrievals and the subsequent VMR retrievals for CO<sub>2</sub>. This included a number of microwindows in the range 1899–1935 cm<sup>-1</sup> (5.17–5.27 μm), a set in the range 2044–2073 cm<sup>-1</sup> (4.82–4.89 μm), and a set in the range 2293–2393 cm<sup>-1</sup> (4.18–4.36 μm). Influence of deviations from LTE is much smaller for an absorption-based instrument like the ACE-FTS than for instruments measuring emission. However, to minimize possible non-LTE effects, all lines used in the analysis originate from the ground vibrational state. Near 2350 cm<sup>-1</sup> (4.25 μm) in particular, care was taken to avoid interferences in the microwindows from lines with excited lower state vibrations, as well as strong lines from subsidiary isotopologues of CO<sub>2</sub> (e.g., <sup>13</sup>CO<sub>2</sub>). CO<sub>2</sub> absorption is calculated using the spectroscopic parameters in the HITRAN 2004 linelist (Rothman et al., 2005).

The ACE-FTS CO<sub>2</sub> observations combining both sunrise and sunset occultations are shown in Fig. 1 and are averages of the period 21 February 2004 to 30 August 2007. The coverage is not uniform and reflects that the SCISAT-1 orbit was optimized to investigate the Arctic stratosphere in winter while obtaining reasonable coverage at lower latitudes. The data indicate a general fall-off of the CO<sub>2</sub> VMR with height in the upper mesosphere and lower thermosphere as may be expected from the loss processes (see below). The meridional CO<sub>2</sub> distribution for the solstice months appears to be consistent with the large-scale circulation exhibited by the extended Canadian Middle Atmosphere Model (CMAM). As reported by McLandress et al. (2006), the meridional wind in the CMAM is characterized by summer-to-winter flow in the mesosphere and winter-to-summer flow in the lower thermosphere, between 100 and 120 km. The former is a feature of the thermally indirect circulation driven primarily by non-orographic gravity wave drag (GWD), whereas the meridional wind reversal in the lower thermo-

## Observations and analysis using the extended CMAM

S. R. Beagley et al.

Title Page

Abstract

Introduction

Conclusions

References

Tables

Figures

◀

▶

◀

▶

Back

Close

Full Screen / Esc

Printer-friendly Version

Interactive Discussion



sphere is a direct result of the resolved wave drag. This circulation pattern suggests that in the MLT subpolar summer region there should be upwelling in the lower and middle mesosphere and downwelling in the upper mesosphere. In agreement with this pattern, the January CO<sub>2</sub> data for the austral subpolar region appear to indicate the upwelling cell up to about 85 km ( $\sim 5 \cdot 10^{-3}$  hPa) and downwelling cell in the region above, where the descending air brings down low CO<sub>2</sub> mixing ratios. This is also hinted at in the June/July data for boreal regions.

To estimate the error on CO<sub>2</sub> VMR retrieved from the ACE-FTS, three sources are considered. The first is the statistical error from the retrieval process. The second contribution comes from uncertainty in the temperature and is estimated by shifting the temperature profile by a common amount of 2 K and repeating the retrieval. Note that atmospheric density (which is inversely proportional to temperature) must also be adjusted in this process to retain internal consistency. The third contribution to the error is derived from the difference between the P/T and VMR retrieval approaches. This represents a limit on the accuracy of the results due to altitude sampling and to interpolation from the measurement grid to the standard 1-km grid used in the forward model calculations for the ACE-FTS. This contribution varies with the altitude spacing between measurements, and is typically larger for larger altitude spacing. The altitude spacing for ACE-FTS measurements varies over the course of a year, ranging from less than 2 km to about 6 km. The estimated errors on CO<sub>2</sub> VMR shown in Fig. 2 use a representative set of occultations with altitude spacing between 3 and 4 km. In global terms, then, the errors are generally less than 10% below 100 km.

Above the mesopause, temperature changes rapidly with altitude, and a temperature uncertainty of 2 K is possibly an underestimate. If this is true, the uncertainty at higher altitudes reported in Fig. 2 have been underestimated. In the P/T retrieval CO<sub>2</sub> VMR is taken as a constant as a function of altitude above  $\sim 125$  km ( $\sim 2 \cdot 10^{-5}$  hPa). This could lead to larger errors at the highest altitudes, but the effect is difficult to quantify and is not explicitly included in the current estimate. Uncertainties in the CO<sub>2</sub> spectroscopic constants from HITRAN 2004 are also excluded from the error estimate.

**Observations and analysis using the extended CMAM**

S. R. Beagley et al.

Title Page

Abstract

Introduction

Conclusions

References

Tables

Figures

◀

▶

◀

▶

Back

Close

Full Screen / Esc

Printer-friendly Version

Interactive Discussion



### 3 Model

For the analysis we have used an enhanced chemistry version of the vertically extended version of the CMAM model (Beagley et al., 2000, 2007; Fomichev et al., 2002; McLandress et al., 2006) with a top at  $2 \times 10^{-7}$  hPa (geopotential height  $\sim 220$  km but dependent on the solar cycle). The model originally contains the non-LTE parameterization for the  $15 \mu\text{m}$   $\text{CO}_2$  band, solar heating due to absorption by  $\text{O}_2$  in the Schumann-Runge bands and continuum, and by  $\text{O}_2$ ,  $\text{N}_2$  and  $\text{O}$  in the extreme ultraviolet spectral region, parameterized chemical heating, molecular diffusion and viscosity and ion drag. The Hines (1997a, b) non-orographic GWD scheme used in the model also includes the impact of turbulence generated by the wave breaking on the momentum budget, thermal diffusion and allows for diffusive transport of minor species; this eddy diffusion we call  $K_{ZZ}(\text{GWD})$ . The model also has a  $K_{ZZ}$  resulting from wind shear and a background value of  $K_{ZZ}$  for numerical control, the sum of both is generally less than  $0.2 \text{ m}^2 \text{ s}^{-1}$ . In addition to the numerical diffusion, tracers in the model experience mixing from resolved dynamical processes such as planetary waves, gravity waves and tides. This resolved diffusion is expected to be realistic. Also above  $\sim 90$  km ( $\sim 0.002$  hPa) vertical diffusive mixing is dominated by molecular diffusion. The model now includes comprehensive stratospheric chemistry (e.g., de Grandpre et al., 2000) with radiatively interactive  $\text{O}_3$  and  $\text{H}_2\text{O}$ , and non-LTE treatment of the near-infrared  $\text{CO}_2$  heating (Ogibalov and Fomichev, 2003). It also has a simplified ion chemistry scheme (Beagley et al., 2007) over a vertically limited domain. The dynamical code has been modified from the earlier version (Beagley et al., 2000; Fomichev et al., 2002; McLandress et al., 2006) to allow for a 7.5 min time step without the previously used upper level enhanced horizontal diffusion being required. These represent the standard conditions and we will explore modifications of the standard conditions below. In the text below, this standard or control run is called scenario A and is listed in Table 1.

The chemistry of  $\text{CO}_2$  in the model is straightforward. It consists of photolysis of  $\text{CO}_2$  from wavelengths between 100–220 nm and  $\text{CO}_2$  is reformed by reaction with OH, viz.

## Observations and analysis using the extended CMAM

S. R. Beagley et al.

Title Page

Abstract

Introduction

Conclusions

References

Tables

Figures

◀

▶

◀

▶

Back

Close

Full Screen / Esc

Printer-friendly Version

Interactive Discussion



$\text{CO} + \text{OH} \rightarrow \text{H} + \text{CO}_2$ . Between  $\sim 65$  km and 95 km the main destruction of  $\text{CO}_2$  is photolysis by Lyman- $\alpha$  with loss in the Schumann-Runge Bands (SRB) being important below 65 km ( $\sim 0.2$  hPa) and in the Schumann-Runge Continuum (SRC) being important above 95 km ( $\sim 5 \cdot 10^{-4}$  hPa) (e.g., Brasseur and Solomon, 1984). Although there is some uncertainty in the  $\text{CO}_2$  cross section at the longer wavelengths which would affect photolysis below 65 km the photolysis in the main region of interest, Lyman- $\alpha$ , is generally well characterized. In any case we discuss the impact of the uncertainties below. CO is formed at all wavelengths with unit efficiency. Below about 45 km ( $\sim 2$  hPa) CO is produced by oxidation of  $\text{CH}_4$ .

In the analysis we shall make use of this intimate connection between CO and  $\text{CO}_2$  in order to provide constraints on the possibilities for agreement between measurements and model. One other point to note is that the model simulations utilized a surface boundary condition of 335 ppmv while the background  $\text{CO}_2$  for the ACE measurements is about 375 ppmv. In order to compare the vertical structures, we have scaled, in the plots, the model CO and  $\text{CO}_2$  values by this ratio to match the observations.

## 4 Results

In the following we compare the ACE measurements with the CMAM results. But first we compare the ACE measurements with other experimental data including both optical and in-situ measurements from CRISTA, SABER and rockets. Figure 3 shows a mean  $\text{CO}_2$  profile based on a compilation of rocket measurements (Fomichev et al., 1998), a global mean of the CRISTA measurements (Kaufmann et al., 2002), a daytime global mean (V1.06) of the SABER measurements (see above) and a global mean of the ACE measurements. Even though there are latitudinal variations in the  $\text{CO}_2$  distribution (Fig. 1) it is clear that these differences are much less than the vertical differences between the various measurements and the model. The CMAM global results indicate a gradual fall-off above 80–85 km and, in general, the rate of fall-off is slower than for all the measurements except for the average rocket profile. However,

### Observations and analysis using the extended CMAM

S. R. Beagley et al.

Title Page

Abstract

Introduction

Conclusions

References

Tables

Figures

◀

▶

◀

▶

Back

Close

Full Screen / Esc

Printer-friendly Version

Interactive Discussion



**Observations and  
analysis using the  
extended CMAM**

S. R. Beagley et al.

above 90 km the rocket measurements fall off more rapidly than the model results. The CRISTA measurements are the lowest with the knee commencing at  $\sim 70$  km ( $\sim 0.1$  hpa) well below the ACE knee of about 78 km. However, above  $\sim 80$  km ( $\sim 0.01$  hPa) the slope of the average CRISTA and ACE results are similar. For the SABER results the knee occurs at  $\sim 80$  km, comparable to ACE measurements, but the SABER curve lies  $\sim 20$  ppmv higher than ACE above the knee. For the rocket measurements the knee lies highest at  $\sim 85$  km ( $\sim 5 \cdot 10^{-3}$  hpa). Clearly there is a discrepancy between the different experiments with ACE and daytime SABER (V1.06) being the closest. As we noted above the derivation of  $\text{CO}_2$  profiles from emissions measurements requires a complex non-LTE model while rocket measurements could be compromised by sampling problems in the vicinity of the rocket skin. ACE measures the ground state of  $\text{CO}_2$  and, hence, provides more reliable information on the  $\text{CO}_2$  abundance.

Figure 4 shows a comparison between the ACE-FTS measurements and the extended CMAM, for April, for various scenarios to be discussed below. Since CMAM is a climate model we cannot compare with the same dates on which the measurements were taken. However, the CMAM data averaged over the month appropriate for the ACE-FTS measurements should be representative. The ACE-FTS gives a reasonable latitudinal coverage in April and from Fig. 4 we see that the overall structure exhibited by the model for the standard scenario, A, is similar to that of the observations. However, the measurements appear to have more structure with latitude. Also, the initial fall-off of  $\text{CO}_2$  mixing ratio with height for the ACE measurements is clearly seen to occur at lower altitudes than for the model results in the control run, scenario A.

Prompted by the disagreement between the model and measurements we have explored the conditions required to produce better agreement between the two. This was undertaken using a series of model sensitivity experiments to explore the processes which might impact the profile in order to reconcile the model and observations. The list of scenarios is given in Table 1 and in more detail in the text following. In an attempt to simulate the knee occurring at lower altitudes we have increased the photolysis rate for  $\text{CO}_2$  by a factor of 5; this is scenario B. As the standard scenario A includes eddy

[Title Page](#)[Abstract](#)[Introduction](#)[Conclusions](#)[References](#)[Tables](#)[Figures](#)[◀](#)[▶](#)[◀](#)[▶](#)[Back](#)[Close](#)[Full Screen / Esc](#)[Printer-friendly Version](#)[Interactive Discussion](#)

diffusion of chemical species associated with parameterized GWD, we introduce a scenario C with  $K_{ZZ}(\text{GWD})$  neglected to explore the impact of mixing by unresolved gravity waves. Scenario D is a simulation that is a combination of B and C, i.e., both an increased photolysis rate for  $\text{CO}_2$  and the neglect of mixing due to  $K_{ZZ}(\text{GWD})$ . In order to explore the contribution of CO recombination to  $\text{CO}_2$ , scenario E assumes a recombination rate for CO and OH to produce  $\text{CO}_2$  five times slower than the standard rate. For completeness, we have also investigated the impact of molecular diffusion and so for scenario F we have eliminated molecular diffusion for  $\text{CO}_2$ ; note that molecular diffusion is retained for all the other species.

The cross-sections for each scenario for the month of April are shown in Fig. 4 and the behaviour is generally what might be expected. Scenario B with the increased J value shows that  $\text{CO}_2$  is depleted in the MLT region compared to A. There is some difference in the structure in the lower thermosphere where the contours are flatter for B. From scenario C it is clear that eddy diffusion effects from GWD do have an impact, transporting  $\text{CO}_2$  up the vertical gradient. The impact of D, i.e. a combination of both B and C, is clearly excessive in terms of reducing the model  $\text{CO}_2$  field in the MLT. For scenario E, the impact of reduced formation of  $\text{CO}_2$  from CO is only seen below  $\sim 0.005$  hPa ( $\sim 85$  km), resulting in less  $\text{CO}_2$ . Scenario F has an impact in the mesosphere resulting in a smaller  $\text{CO}_2$  field. In the lower thermosphere the  $\text{CO}_2$  field is increased as it is maintained by the resolved wind field and is not constrained by trying to achieve gravity-diffusive equilibrium with a concomitantly smaller scale height.

Figure 5 shows a series of averaged ACE April profiles for regions where there is ample ACE data, viz.,  $\sim 30^\circ$  N,  $3^\circ$  N and  $80^\circ$  S respectively. Also shown are the CMAM profiles for the various scenarios listed in Table 1 which highlights more clearly the inability of the model to simulate the height at which the  $\text{CO}_2$  mixing ratio begins to fall off as shown by the ACE data. At  $30^\circ$  N for April (Fig. 5a) the ACE mixing ratio data indicate a distinct fall-off or knee beginning at  $\sim 80$  km. All the model results indicate a fall-off in this region but it is not as steep. Clearly the scenario which gives the best agreement is one where the J value is increased by a factor of five B while the

**Observations and analysis using the extended CMAM**

S. R. Beagley et al.

Title Page

Abstract

Introduction

Conclusions

References

Tables

Figures

◀

▶

◀

▶

Back

Close

Full Screen / Esc

Printer-friendly Version

Interactive Discussion



worst agreement above 100 km ( $\sim 1.10^{-4}$  hPa), as might be expected, is F i.e. with no molecular diffusion. Only D, with both high J value and no  $K_{ZZ}$  from GWD, lies below the measurements.

Figure 5b shows the same comparison as 30° N for the tropics (3° N) for April and the results are generally the same with the increased J value giving the best agreement with the other scenarios generally following those seen in Fig. 5a. For austral polar regions (80° S) the results are shown in Fig. 5c. For this case none of the scenarios provide good agreement. Even scenario B, is a poor fit and scenario D, with modified J and  $K_{ZZ}(\text{GWD})=0$  is too low. Viewed as an experiment on the role of GWD this suggests that perhaps the  $K_{ZZ}$  generated by the GWD parameterization is strongest in the polar autumnal region so that the  $\text{CO}_2$  is diffused up the gradient to higher altitudes. This is confirmed by Fig. 6 that shows a zonally and temporally average  $K_{ZZ}(\text{GWD})$  for the month of April. It is clearly seen that the impact of turbulence generated by unresolved gravity wave breaking on the model mixing is most important in polar regions where  $K_{ZZ}(\text{GWD})$  is by about an order of magnitude larger than in the tropical and mid-latitude regions.

Figure 7 shows the April CO mixing ratios for ACE and for each of the scenarios for CMAM shown in Table 1. The standard scenario, A, suggests that the CMAM simulation of CO provides a reasonable representation of CO. This is not unexpected as the standard CMAM with a top at 0.001 hPa also simulates well the CO distribution (Jin et al., 2005, 2008). At all latitudes the extended CMAM model CO, scenario A, is generally within 30% of the ACE CO, which, considering the rapid vertical variation of CO seems quite reasonable. However, we should bear in mind that the CO production rate calculated from the photolysis of  $\text{CO}_2$  must be too high above 80 km since the model  $\text{CO}_2$  field is too high for the control run (A).

It also appears that the ACE polar data suggest strong descent at  $\sim 70^\circ$  S with slower descent over the pole. However, this is an artifact due to the sampling limitations of the ACE experiment during a time of strong descent. For example at  $85^\circ$  S the sampling occurs about a month ahead of the latitudes sampled at  $70^\circ$  S and with monthly aver-

**Observations and analysis using the extended CMAM**

S. R. Beagley et al.

Title Page

Abstract

Introduction

Conclusions

References

Tables

Figures

◀

▶

◀

▶

Back

Close

Full Screen / Esc

Printer-friendly Version

Interactive Discussion



**Observations and  
analysis using the  
extended CMAM**

S. R. Beagley et al.

aging this appears as localized descent  $\sim 70^\circ$  S (compare Fig. 13 of Jin et al., 2008). For scenario B with increased J value we see that the CO is up to a factor of five too large at most locations and this is with a  $\text{CO}_2$  distribution which fits the ACE observations; one implication is that the removal process for  $\text{CO}_2$  cannot simply result in production of CO. For case C with  $K_{ZZ}(\text{GWD})$  turned off the model CO is too low by  $\sim 30\%$  at 0.002 hPa ( $\sim 90$  km) but at 0.2 hPa ( $\sim 65$  km) the model is too high by about 30% as compared to the ACE, so that the gradient has been affected by turning off  $K_{ZZ}(\text{GWD})$  (see below). For case D the model CO is too high by about a factor of 4 which suggests that this scenario is also not reasonable. For case E, where the CO loss has been reduced, above about 0.01 hPa ( $\sim 80$  km) the CO is only slightly larger than the standard scenario, A, reflecting that the CO in this region is largely controlled by dynamics whereas below  $\sim 80$  km the larger CO VMRs reflect the slower loss process as compared to case A. For case F with molecular diffusion turned off for  $\text{CO}_2$  the CO increases in the upper part of the domain reflecting higher  $\text{CO}_2$  concentration in the lower thermosphere. Incidentally, the results in this case are in good agreement with the observations, but this has resulted for the wrong reasons as a consequence of unrealistically high thermospheric  $\text{CO}_2$ .

Similar to Fig. 5, Fig. 8 shows profile data for ACE and CMAM CO at latitudes where there is adequate data,  $30^\circ$  N,  $3^\circ$  N and  $80^\circ$  S respectively. The CMAM data are for the scenarios listed in Table 1. The standard CO profile is in reasonable agreement with the ACE data below 0.01 hPa ( $\sim 80$  km); above this height it is lower than the observations and is 30% too low by  $1.10^{-4}$  hPa ( $\sim 98$  km) for these latitudes. Case B with increased photolysis is too large by a factor between 4 and 5, varying with height. Given that the model  $\text{CO}_2$  is in reasonable agreement with the observations for this case, this suggests that the CO source is too large by about a factor of 5. This strongly suggests that increased photolysis cannot solve the problem and is thus an important constraint. Scenario C with decreased  $K_{ZZ}$  is in reasonable agreement with the observations (but of course the  $\text{CO}_2$  does not fit). This CO profile is larger than that for scenario A since the downward diffusion has been decreased with  $K_{ZZ}(\text{GWD})=0$ . Scenario D is perhaps

Title Page

Abstract

Introduction

Conclusions

References

Tables

Figures

◀

▶

◀

▶

Back

Close

Full Screen / Esc

Printer-friendly Version

Interactive Discussion



**Observations and  
analysis using the  
extended CMAM**

S. R. Beagley et al.

Title Page

Abstract

Introduction

Conclusions

References

Tables

Figures

◀

▶

◀

▶

Back

Close

Full Screen / Esc

Printer-friendly Version

Interactive Discussion



the worst case and the disagreement of scenario B is amplified by the reduction of downward diffusion due to  $K_{ZZ}$ . For scenario E the VMRs reflect the slower CO loss rate so that the model mixing ratios are too large below about 0.005 hPa ( $\sim 85$  km). The effect of zeroing molecular diffusion for  $\text{CO}_2$  (scenario F) increases CO due to larger VMRs of  $\text{CO}_2$  in the lower thermosphere. For the tropics the comparison is similar. Scenarios B and D produce CO mixing ratios that are much too large compared to the ACE observations. The other scenarios are generally too low above about 80 km. For the austral polar region, similar behaviour is exhibited as for the other latitudes. It should be noted that none of the model results give agreement below 0.1 hPa ( $\sim 70$  km) and the standard run is too small by a factor of 2 at  $\sim 0.001$  hPa ( $\sim 92$  km).

The above has focused on vernal equinox. We now investigate the late northern summer, August, to ensure that the same characteristics prevail for all seasons. August is a month where the ACE data has adequate coverage from the northern sub-tropics to the austral polar regions. Figure 9 shows the ACE  $\text{CO}_2$  data for August and the CMAM data for the scenarios discussed above and shown in Table 1 (scenario E is not included for August). A comparison of the ACE data with the standard scenario, A, shows that the behaviour is similar in August as for April in that the measured  $\text{CO}_2$  begins to fall off at lower altitudes than does the model. We note that the slopes of the ACE contours in the polar region are affected by sampling as for April as can also be seen in Jin et al. (2008). However, there are qualitative differences between April and August for the other scenarios. For example, scenario B with an increased J value is now excessive, in that the CMAM  $\text{CO}_2$  falls off too rapidly in this case. Scenario C with  $K_{ZZ}$ (GWD) turned off produces results where  $\text{CO}_2$  is too high while for scenario D, the combination of B and C,  $\text{CO}_2$  is excessive as for the April results. And scenario F with molecular diffusion turned off clearly shows the importance of molecular diffusion. We have also looked at the plots (not shown) for specific latitudes as for April and the above behaviour is confirmed.

In Fig. 10 we present the plots for August for CO for ACE data and the Table 1 scenarios of CMAM. The control scenario, A, gives quite good agreement below about

0.05 hPa ( $\sim 75$  km) but is about a factor of 2 low at 0.001 hPa ( $\sim 92$  km) and the latitudinal behaviour is quite similar. For scenario B, the CO is generally too high by up to a factor of five which again suggests that an increased J value is not the solution for the poor fit for the control. Scenario C with a decreased  $K_{ZZ}$  leads to an even poorer fit at  $\sim 0.001$  hPa as the CO is not diffused down as rapidly while the agreement remains reasonable at  $\sim 1$  hPa since the distribution is controlled by chemistry. Scenario D is, as expected, poorer than either B or C. Similar to the results for April, case F gives reasonable CO concentrations in the upper part of the domain that, however, reflects unrealistically high CO<sub>2</sub> concentration in the lower thermosphere.

## 5 Discussion

As far as we can discern this is the first published 3-D study of CO<sub>2</sub> in the MLT region using a GCM with a vertical domain that extends from the surface to the thermosphere. As noted above, Kaufmann et al. (2002) presented a 3-D study of CO<sub>2</sub> using the TIME-GCM. This is a 3-D time dependent GCM extending from 30 to 500 km, and for their calculations they used a  $5^\circ \times 5^\circ$  horizontal resolution with two grid points per scale height in the vertical and a 4 min time step (see for example Roble (1995) and references therein for a more detailed description for the TIME-GCM). Kaufmann et al. (2002) found problems, similar to what we have elucidated above, with the differences of the vertical distributions of CO<sub>2</sub> mixing ratio between measurements and model. Mertens et al. (2008) find similar discrepancies between the SABER V1.06 CO<sub>2</sub> profiles and the TIME-GCM. Chabrilat et al. (2002) have used a 2-D model to investigate the impact of molecular diffusion on the CO<sub>2</sub> distribution in the MLT region. They obtained reasonable agreement with the rocket measurements but did not explicitly compare with the CRISTA measurements which have a knee much lower.

The figures presented above explore a series of sensitivity tests to examine the major processes which affect the CO<sub>2</sub> vertical profile. It is clear that the model can only reproduce a fall-off similar to that seen in ACE when the photolysis is increased sig-

### Observations and analysis using the extended CMAM

S. R. Beagley et al.

Title Page

Abstract

Introduction

Conclusions

References

Tables

Figures

◀

▶

◀

▶

Back

Close

Full Screen / Esc

Printer-friendly Version

Interactive Discussion



**Observations and  
analysis using the  
extended CMAM**

S. R. Beagley et al.

Title Page

Abstract

Introduction

Conclusions

References

Tables

Figures

◀

▶

◀

▶

Back

Close

Full Screen / Esc

Printer-friendly Version

Interactive Discussion

nificantly, far beyond any reasonable uncertainty in the known parameters determining the photolysis in this region. Other factors such as the magnitude of turbulence generated by breaking of the unresolved gravity waves, uncertainties in the  $\text{CO}_2$  reformation rates and the action of molecular diffusion at this altitude seem unable to produce the correct change in distribution of the  $\text{CO}_2$ . We note that the application of  $K_{ZZ}(\text{GWD})$  is not a standard feature of middle atmosphere models. To our best knowledge, there are only two GWD parameterizations (Hines, 1997a,b; Lindzen, 1981) which provide eddy diffusion coefficients. That is why we have investigated the impact of  $K_{ZZ}(\text{GWD})$  removal. In addition, the resolved circulation in the middle atmosphere is quite sensitive to the tuning of GWD parameterizations and this can also affect the species distribution as much as  $K_{ZZ}(\text{GWD})$ . Given the uncertainty in our knowledge of the effects of diffusion generated by gravity wave breaking, a major contributor to the  $K_{ZZ}$  in this region, some concern over the role and strength of gravity wave induced motion is warranted. However, even if we neglect all diffusive transport associated with unresolved gravity wave breaking, the  $\text{CO}_2$  vertical profile does not begin to fall off in the model as low as the ACE observations indicate. Nevertheless we note that for other species in the MLT region, such as  $\text{H}_2\text{O}$ ,  $\text{N}_2\text{O}$ ,  $\text{CH}_4$ , as well as  $\text{CO}_2$ , for which their distributions are determined by vertical transport balanced by chemical loss, that knowledge of  $K_{ZZ}$  is important in the determination of their distributions (see also Jin et al., 2008).

Although the photolysis rate of  $\text{CO}_2$  appears reasonably well characterized, except, as noted above, at longer wavelengths, we have estimated what increase might be required to produce agreement (without consideration of CO): this is scenario B. This scenario appears to be the only simulated process capable of reconciling the model and observations amongst the scenarios considered. Although, based on the current knowledge, we could not find any physical reasons for the  $\text{CO}_2$  photolysis to be a few times larger than that used in scenario A; results from scenario B clearly indicate that some additional  $\text{CO}_2$  loss processes are required in the mesosphere in order to reconcile the model and observations.

In the height region of interest, between approximately 70 and 100 km ( $\sim 0.1-$

**Observations and  
analysis using the  
extended CMAM**

S. R. Beagley et al.

1.10<sup>-4</sup> hPa), the CO<sub>2</sub> molecule is photolyzed mainly in the Lyman- $\alpha$  line. In this case the value of the photolysis rate depends on CO<sub>2</sub> and O<sub>2</sub> cross sections in the vicinity of Lyman- $\alpha$  and on the level of solar activity. The solar flux in the Lyman- $\alpha$  line varies by about 30% from solar maximum to solar minimum. However, for the period of the ACE observations (2004–2007), the solar irradiance at Lyman- $\alpha$  line reported on the SOLARIS website ([http://www.geo.fu-berlin.de/en/met/ag/strat/research/SOLARIS/Input\\_data](http://www.geo.fu-berlin.de/en/met/ag/strat/research/SOLARIS/Input_data)) does not differ by more than 10% from that used in our calculation, with our value being generally larger.

The CO<sub>2</sub> cross section at Lyman- $\alpha$  for about 300K reported by different authors varies between (6.5–8.2)×10<sup>-20</sup> cm<sup>2</sup> (e.g. see Yoshino et al., 1996). There is also a weak temperature dependence: the cross section slowly increases with temperature at 0.1%/K (Lewis and Carver, 1983). Some uncertainties exist in what temperature the cross section should be taken at. The kinetic temperature in the upper mesosphere is generally lower than 200K. However, there is some justification for higher temperatures being used. This is because the vibrational levels of CO<sub>2</sub> are non-thermally excited in the mesosphere so that daytime vibrational temperatures are higher than the kinetic temperature (e.g., López-Puertas and Taylor, 2001). However, this cannot likely explain a considerable increase in the CO<sub>2</sub> photolysis rate. Daytime vibrational temperatures do not exceed 250 K and 350 K for the lower and higher vibrational levels, respectively (e.g., López-Puertas and Taylor, 2001). Given the temperature dependence of the CO<sub>2</sub> cross section to be 0.1%/K, the latter means that non-thermal excitation of the CO<sub>2</sub> vibrational levels cannot lead to a cross section increase of more than ~5% from the value measured at 300 K.

Chabrillat and Kockarts (1997) have noted that because of the structure in the O<sub>2</sub> absorption cross section in the vicinity of Lyman- $\alpha$  that J values for H<sub>2</sub>O and CH<sub>4</sub> are affected to varying degrees. Thus we have evaluated the impact on J(CO<sub>2</sub>) and find that its uncertainty is less than 15% in the height region of interest so that its contribution to the uncertainty is much less than is required by our comparisons. Also J(CO<sub>2</sub>) is rather uncertain at longer wavelengths both versus wavelength and temperature (Parkinson

Title Page

Abstract

Introduction

Conclusions

References

Tables

Figures

◀

▶

◀

▶

Back

Close

Full Screen / Esc

Printer-friendly Version

Interactive Discussion



et al., 2003; Shemansky, 1972; Karaiskou et al., 2004). However this long wavelength uncertainty should only affect  $J(\text{CO}_2)$  for altitudes below about 65 km ( $\sim 0.2$  hPa) (see, for example, Brasseur and Solomon, 1984) and not impact our calculations. For the  $\text{CO}_2$  cross section in the Lyman- $\alpha$  region we use a value of  $7.7 \times 10^{-20} \text{ cm}^2$  which suggests that even with all the uncertainties taken into account, we rather overestimate the  $\text{CO}_2$  photolysis rate in the upper mesosphere than underestimate it.

CO provides an important additional constraint on the problem of the carbon distribution in the MLT region. CO is created from the  $\text{CO}_2$  photolysis and is advected and diffused from above. In the control model simulation, scenario A, CMAM CO is up to a factor of two too low above  $\sim 0.01$  hPa ( $\sim 80$  km) but it is not clear how serious a disagreement this is. But even though the source,  $\text{CO}_2$ , is too high and the J value should be appropriate the CO is low. As noted above there is no clear evidence to suggest a serious error in the photolysis rate of  $\text{CO}_2$  at these altitudes. A number of the sensitivity experiments do create higher CO levels at the pressure range required to mimic the ACE observations, viz., scenarios B (enhanced photolysis of  $\text{CO}_2$ ), C (reduced  $K_{ZZ}$ ), and F (molecular diffusion=0) as can be seen from Figs. 7 and 8. A change in  $K_{ZZ}$  could be envisaged to get CO closer to the ACE observations but a neglect of molecular diffusion (namely no gravitational separation of  $\text{CO}_2$ ) is physically unreasonable. And, as we have seen in Figs. 7, 8 and 10, the J value enhancement results indicate that the concomitant increase in CO is too large compared to the ACE observations. For this scenario B the agreement between measured and modelled CO has worsened above 65 km with the source of CO having increased dramatically and unrealistically.

The impact of scenario C ( $K_{ZZ}(\text{GWD})=0$ ) is to effect a fall-off in  $\text{CO}_2$  at lower altitudes as the upward transport of  $\text{CO}_2$  down the mixing ratio gradient has been decreased. We note that the agreement between model and measurements is improved somewhat but that the model  $\text{CO}_2$  still remains too high. Although the experiments with reduced  $K_{ZZ}(\text{GWD})$  are not the solution to the current discrepancy between the ACE observations and model they are, however, revealing. It is clear that the Hines GWD induced  $K_{ZZ}$  may play an important role in the vertical transport of species in the mesosphere

**Observations and analysis using the extended CMAM**

S. R. Beagley et al.

Title Page

Abstract

Introduction

Conclusions

References

Tables

Figures

◀

▶

◀

▶

Back

Close

Full Screen / Esc

Printer-friendly Version

Interactive Discussion



for some species such as CO, NO, CH<sub>4</sub>, N<sub>2</sub>O, H<sub>2</sub>O as well as CO<sub>2</sub> but its vertical and latitudinal structure has not been thoroughly explored. It would be interesting to investigate the impact of K<sub>zz</sub> fields derived from other GWD schemes. As noted above each GWD scheme will induce not just a different dynamical and temperature structure but also a different species structure and by choosing suitable species it may be possible to further constrain GWD parameterizations.

As is clear from above results the most reasonable scenario for agreement between the ACE observations and CMAM simulations is with an increased J value (perhaps with a different enhancement factor between April and August). However, the concomitant increased source of CO is not present in the observations. This is then suggestive that carbon may be sequestered elsewhere in the atmospheric system. At this point our only suggestion is perhaps CO<sub>2</sub> may react with meteoritic dust in the mesosphere. Estimating reaction times at ~80 km using typical meteoritic surface areas (e.g., Megner et al., 2008) we obtain 9/γ hours where γ is the efficiency for non-reversible reaction on the dust, this should be compared with 1/J(CO<sub>2</sub>) for Lyman-α at 80 km which is ~13 days for a diurnal average at mid-latitudes. Thus γ=0.1 would yield a loss process ~3–5 times faster than photolysis This could yield a faster CO<sub>2</sub> removal rate while not producing CO. If this in fact proves to be the case then one might expect other similar reactions to be occurring on meteoritic dust. An interesting feature of such a phenomenon is that it will be sporadic, and its effects will vary from season to season with varying dust amounts which might account for the variation required in the “enhanced” J (CO<sub>2</sub>) to account for the observations in April and August.

One of the issues that might be of importance to consider is how well the extended CMAM simulates temperatures. With this in mind we present zonally and temporarily averaged latitude-pressure temperature for ACE and the CMAM control run in Fig. 11a for April and in Fig. 11b for August. Bearing in mind that there are sampling limitations for ACE the agreement between temperatures are rather good.

**Observations and analysis using the extended CMAM**

S. R. Beagley et al.

Title Page

Abstract

Introduction

Conclusions

References

Tables

Figures

◀

▶

◀

▶

Back

Close

Full Screen / Esc

Printer-friendly Version

Interactive Discussion



## 6 Summary

We present the first global set of observations of ground state CO<sub>2</sub> for the mesosphere and lower thermosphere. We also present the measurements of CO obtained concurrently. They were obtained by the ACE-FTS instrument on SCISAT-I, a small Canadian satellite, using solar occultation. There are certain limitations on seasonal and zonal averages due to the particular orbit which emphasizes investigations of polar regions and also due to the particular sampling properties of solar occultation. The CO<sub>2</sub> mixing ratio distribution from ACE lies between the CRISTA values (Kaufmann et al., 2002) and the rocket values, (compilation by Fomichev et al., 1998), and is similar to the SABER V1.06 measurements (Mertens et al., 2009).

We have compared the ACE measurements to calculations of the CO<sub>2</sub> and CO distributions using a version of the Canadian Middle Atmosphere Model (CMAM) which has been vertically extended to about 220 km. Applying standard chemistry we find that we cannot get agreement between the ACE observations and CMAM simulations in the mesosphere and in particular, the model cannot reproduce adequately the height of the knee, i.e. the height at which CO<sub>2</sub> begins to fall off while adequately reproducing the CO observations. We have investigated the variation of several parameters of interest in order to explore parameter space for this problem. Our conclusions are that there must be a loss process for CO<sub>2</sub> that will sequester the carbon in some form other than CO; we have speculated on the role of meteoritic dust. We also highlight the important role for K<sub>ZZ</sub>, viz. eddy diffusion of species associated with GWD.

*Acknowledgements.* The authors would like to thank the Canadian Space Agency (CSA), the Natural Sciences and Engineering Research Council (NSERC) of Canada, the Canadian Foundation for Climate and Atmospheric Science (CFCAS), the Canadian Foundation for Innovation, the Ontario Innovation Trust for support and the UK Natural Environment Research Council.

ACPD

9, 11551–11587, 2009

### Observations and analysis using the extended CMAM

S. R. Beagley et al.

Title Page

Abstract

Introduction

Conclusions

References

Tables

Figures

◀

▶

◀

▶

Back

Close

Full Screen / Esc

Printer-friendly Version

Interactive Discussion



## References

- Beagley, S. R., McLandress, C., Fomichev, V. I., and Ward, W. E.: The Extended Canadian Middle Atmosphere Model, *Geophys. Res. Lett.*, 27(16), 2529–2532, 2000.
- Beagley, S. R., McConnell, J. C., Fomichev, V. I., Semeniuk, K., Jonsson, A. I., Garcia Munoz, A., McLandress, C., and Shepherd, T. G.: Extended CMAM: Impacts of thermospheric neutral and ion chemistry on the middle atmosphere, AGU, fall, 2007.
- Bernath, P. F., McElroy, C. T., Abrahams, M. C., Boone, C. D., Butler, M., Camy-Peyret, C., Carleer, M., Clerbaux, C., Coheur, P.F., Colin, R., DeCola, P., DeMazire, M., Drummond, J. R., Dufour, D., Evans, W. F. J., Fast, H., Fussen, D., Gilbert, K., Jennings, D. E., Llewellyn, E. J., Lowe, R. P., Mahieu, E., McConnell, J. C., McHugh, M., McLeod, S. D., Michaud, R., Midwinter, C., Nassar, R., Nichitiu, F., Nowlan, C., Rinsland, C. P., Rochon, Y. J., Rowlands, N., Semeniuk, K., Simon, P., Skelton, R., Sloan, J. J., Soucy, M.-A., Strong, K., Tremblay, P., Turnbull, D., Walker, K. A., Walkty, I., Wardle, D. A., Wehrle, V., Zander, R., and Zou, J.: Atmospheric Chemistry Experiment(ACE): Mission overview, *Geophys. Res. Lett.*, 32, L15S01, doi:10.1029/2005GL022386, 2005.
- Boone, C. D., Nassar, R., Walker, K. A., Rochon, Y., McLeod, S. D., Rinsland, C. P., and Bernath, P. F.: Retrievals for the atmospheric chemistry experiment Fourier-transform spectrometer, *Appl. Opt.*, 44(33), 7218–7231, 2005.
- Brasseur, G. and Solomon, S.: *Aeronomy of the Middle Atmosphere*, D. Reidel, 441 pp., 1984.
- Chabrilat, S. and Kockarts, G.: Simple parameterization of the absorption of the solar Lyman-alpha line, *Geophys. Res. Lett.*, 24, 2659–2662, 1997.
- Chabrilat, S., Kockarts, G., Fonteyn, D., and Brasseur, G.: Impact of molecular diffusion on the CO<sub>2</sub> distribution and the temperature in the mesosphere, *Geophys. Res. Lett.*, 29, 1729, doi:10.1029/2002GL015309 2002.
- de Grandpré, J., Beagley, S. R., Fomichev, V. I., Griffioen, E., McConnell, J. C., Medvedev, A. S., and Shepherd, T. G.: Ozone climatology using interactive chemistry: Results from the Canadian Middle Atmosphere Model, *J. Geophys. Res.*, 105(D21), 26475–26492, doi:10.1029/2000JD900427, 2000.
- Fomichev, V. I., Blanchet, J.-P., and Turner, D. S.: Matrix parameterization of the 15 μm CO<sub>2</sub> band cooling in the middle and upper atmosphere for variable CO<sub>2</sub> concentration, *J. Geophys. Res.*, 103, 11505–11528, 1998.
- Fomichev, V. I., Ward, W. E., Beagley, S. R., McLandress, C., McConnell, J. C., McFar-

ACPD

9, 11551–11587, 2009

## Observations and analysis using the extended CMAM

S. R. Beagley et al.

Title Page

Abstract

Introduction

Conclusions

References

Tables

Figures

◀

▶

◀

▶

Back

Close

Full Screen / Esc

Printer-friendly Version

Interactive Discussion



**Observations and  
analysis using the  
extended CMAM**

S. R. Beagley et al.

Title Page

Abstract

Introduction

Conclusions

References

Tables

Figures

◀

▶

◀

▶

Back

Close

Full Screen / Esc

Printer-friendly Version

Interactive Discussion



lane, N. A., and Shepherd, T. G.: Extended Canadian Middle Atmosphere Model: Zonal-mean climatology and physical parameterizations, *J. Geophys. Res.*, 107(D10), 4087, doi:10.1029/2001JD000479, 2002.

Girard, A., Besson, J., Brard, D., Laurent, J., Lemaitre, M. P., Lippens, C., Muller, C., Vercheval, J., and, Ackerman, M.: Global results of grille spectrometer experiment on board Spacelab 1, *Planet. Space Sci.*, 36, 291–300, 1988.

Hines, C. O.: Doppler-spread parameterization of gravity-wave momentum deposition in the middle atmosphere. Part 1: Basic formulation, *J. Atmos. Sol.-Terr. Phys.*, 59, 371–386, 1997a.

Hines, C. O.: Doppler-spread parameterization of gravity-wave momentum deposition in the middle atmosphere. Part 2: Broad and quasi-monochromatic spectra, and implementation, *J. Atmos. Sol.-Terr. Phys.*, 59, 387–400, 1997b.

Jin, J. J., Semeniuk, K., Beagley, S. R., Fomichev, V. I., Jonsson A. I., McConnell, J. C., Urban, J., Murtagh, D., Manney, G. L., Boone, C. D., Bernath, P. F., Walker, K. A., Barret, B., Ricaud, P., and Dupuy, E.: Comparison of CMAM simulations of CO (CO), nitrous oxide (N<sub>2</sub>O), and methane (CH<sub>4</sub>) with observations from Odin/SMR, ACE-FTS, and Aura/MLS, *Atmos. Chem. Phys. Discuss.*, 8, 13063–13123, 2008, <http://www.atmos-chem-phys-discuss.net/8/13063/2008/>.

Jin, J. J., Semeniuk, K., Jonsson, A. I., Beagley, S. R., McConnell, J. C., Boone, C. D., Walker, K. A., Bernath, P. F., Rinsland, C. P., Dupuy, E., Ricaud, P., De la Noe, J., Urban, J., and Murtagh, D.: A comparison of co-located ACE-FTS and SMR stratospheric-mesospheric CO measurements during 2004 and comparison with a GCM, *Geophys. Res. Letts*, 32, L15S03, doi:10.1029/2005GL022433, 2005.

Karaiskou, A., Vallance, C., Papadakis, V., Vardavas, I. M., and Rakitzis, T. P.: Absolute absorption cross-section measurements of CO<sub>2</sub> in the ultraviolet from 200 to 206 nm at 295 and 373 K, *Chem. Phys. Lett.*, 400, 30–34, 2004.

Kaufmann, M., Gusev, O. A., Grossmann K. U., Roble, R. G., Hagan, M. E., Hartsough, C., and Kutepov, A. A.: The vertical and horizontal distribution of CO<sub>2</sub> densities in the upper mesosphere and lower thermosphere as measured by CRISTA, *J. Geophys. Res.*, 107(D23), 8182, doi:10.1029/2001JD000704, 2002.

Kaye, J. A. and Miller, T. L.: The ATLAS series of shuttle missions, *Geophys. Res. Lett.*, 23, 2285–2288, 1996.

Kumer, J. B., Stair Jr., A. T., Wheeler, N., Baker, K. D., and Baker, D. J.: Evidence for an

$\text{OH}^\ddagger \xrightarrow{h\nu} \text{N}_2^\ddagger \xrightarrow{h\nu} \text{CO}_2 (v_3) \longrightarrow \text{O}_2 + h\nu (4.3 \mu\text{m})$  mechanism for 4.3- $\mu\text{m}$  airglow, J. Geophys. Res., 83, 4743–4747, 1978.

Lewis, B. R. and Carver, J. H.: Temperature dependence of the carbon dioxide photoabsorption cross section between 1200 and 1970 Å, J. Quant. Spectrosc. Radiat. Trans., 30, 297–309, 1983.

Lindzen R. S.: Turbulence and stress owing to gravity wave and tidal breakdown. J. Geophys. Res., 86, 9704–9714, 1981.

López-Puertas, M. and Taylor, F. W.: Non-LTE Radiative Transfer in the Atmosphere. World Scientific, Singapore/New Jersey/London/Hong Kong, 487 pp., 2001.

López-Puertas, M. and Taylor, F. W.: Carbon dioxide 4.3  $\mu\text{m}$  emission in the Earth's atmosphere: A comparison between NIMBUS 7 SAMS measurements and non-local thermodynamic equilibrium radiative transfer calculations, J. Geophys. Res., 94, 13045–13068, 1989.

López-Puertas, M., Zaragoza, G., López-Valverde, M. Á., and Taylor, F. W.: Non local thermodynamic equilibrium (LTE) atmospheric limb emission at 4.6  $\mu\text{m}$  2, An analysis of the daytime wideband radiances as measured by UARS improved stratospheric and mesospheric sounder, J. Geophys. Res., 103, 8515–8530, 1998.

McLandsess, C., Ward, W. E., Fomichev, V. I., Semeniuk, K., Beagley, S. R., McFarlane, N. A., and Shepherd, T. G.: Large-scale dynamics of the mesosphere and lower thermosphere: An analysis using the extended Canadian Middle Atmosphere Model, J. Geophys. Res., 111, D17111, doi:10.1029/2005JD006776, 2006.

Megner, L., Siskind, D. E., Rapp, M., and Gumbel, J.: Global and temporal distribution of meteoric smoke: A two-dimensional simulation study, J. Geophys. Res., 113, D03202, doi:10.1029/2007JD009054, 2008.

Mertens, C. J., Winick, J. R., Picard, R. H., Evans, D. S., López-Puertas, M., Wintersteiner, P. P., Xu, X., Mlynczak, M. G., and Russell III, J. M.: Influence of solar-geomagnetic disturbances on SABER measurements of 4.3  $\mu\text{m}$  emission and the retrieval of kinetic temperature and carbon dioxide, Adv. Space Res., 43, 1325–1336, 2009.

Mertens, C. J., Russell, J. M., Mlynczak, M. Y., She, C.-Y., Schmidlin, F. J., Goldberg, R. A., López-Puertas, M., Wintersteiner, P. P., Picard, R. H., Winick, J. R., and Xu, X.: Kinetic temperature and carbon dioxide from broadband infrared limb emission measurements taken from the TIMED/SABER instrument, Adv. Space Res., 43, 15–27, 2009.

Nebel, H., Wintersteiner, P. P., Picard, R. H., Winick, J. R., Sharma, and R. D.: CO<sub>2</sub> non-local thermodynamic equilibrium radiative excitation and infrared dayglow at 4.3  $\mu\text{m}$ : Application

## Observations and analysis using the extended CMAM

S. R. Beagley et al.

Title Page

Abstract

Introduction

Conclusions

References

Tables

Figures

◀

▶

◀

▶

Back

Close

Full Screen / Esc

Printer-friendly Version

Interactive Discussion



- to spectral infrared rocket experiment data, *J. Geophys. Res.*, 99, 10409–10419, 1994.
- Offermann, D. and Grossmann, K. U.: Thermospheric density and compositions as determined by a mass spectrometer with cryo ion source, *J. Geophys. Res.*, 78, 8296–8304, 1973.
- Offermann, D., Friedrich, V., Ross, P., and Von Zahn, U.: Neutral gas composition measurements between 80 and 120 km, *Planet. Space Sci.*, 29, 747–764, 1981.
- Ogibalov V. P. and Fomichev, V. I.: Parameterization of solar heating by the near IR CO<sub>2</sub> bands in the mesosphere, *Adv. Space Res.*, 32, 759–764, 2003.
- Parkinson, W. H., Rufus, J., and Yoshino, K.: Absolute absorption cross section measurements of CO<sub>2</sub> in the wavelength region 163–200 nm and the temperature dependence, *Chem. Phys.*, 290, 251–256, 2003.
- Philbrick, C. R., Faucher, G. A., and Trzcinski, E.: Rocket measurements of mesospheric and lower thermospheric composition, *Space Res.*, 13, 255–260, Akademie, Berlin, Germany, 1973.
- Remsberg, E. E., Marshall, B. T., Garcia-Comas, M., Krueger, D., Lingenfelter, G. S., Martin-Torres, J., Mlynczak, M. G., Russell III, J. M., Smith, A. K., Zhao, Y., Brown, C., Gordley, L. L., López-Gonzalez, M. J., López-Puertas, M., She, C.-Y., Taylor, M. J., and Thompson, R. E.: Assessment of the quality of the Version 1.07 temperature-versus-pressure profiles of the middle atmosphere from TIMED/SABER, *J. Geophys. Res.*, 113, D17101, doi:10.1029/2008JD010013, 2008.
- Rinsland, C., Gunson, M. R., Zander, R., and López-Puertas, M.: Middle and upper atmosphere pressure-temperature profiles and the abundances of CO<sub>2</sub> and CO in the upper atmosphere from ATMOS/Spacelab 3 observations, *J. Geophys. Res.*, 97, 20479–20495, 1992.
- Roble, R. G.: Energetics of the mesosphere and thermosphere, the upper mesosphere and lower thermosphere: A review of experiment and theory, *AGU Monograph*, 87, 1995.
- Rothman, L. S., Jacquemart, D., Barbe, A., Benner, C. C., Birk, M., Brown, L. R., Carleer, M. R., Chackerian Jr., C., Chance, K., Coudert, K. H., Dana, V., Devi, V. M., Flaud, J.-M., Gamache, R. R., Goldman, A., Hartmann, J. -M., Jucks, K. W., Maki, A. G., Mandin, J. -Y., Massie, S. T., Orphal, J., Perrin, A., Rinsland, C. P., Smith, M. A. H., Tennyson, J., Tolchenov, R. N., Toth, R. A., Vander Auwera, J., Varanasi, P., and Wagner, G.: The HITRAN 2004 molecular spectroscopic database, *J. Quant. Spectr. Radiat. Trans.*, 96, 139–204, 2005.
- Schmidt, H., Brasseur, G. P., Charron, M., Manzini, E., Giorgetta, M. A., Diehl, T., Fomichev, V. I., Kinnison, D., Marsh, D., and Walters, S.: The HAMMONIA chemistry climate model: Sensitivity of the mesopause region to the 11-year solar cycle and CO<sub>2</sub> doubling, *J. Climate*,

**Observations and analysis using the extended CMAM**

S. R. Beagley et al.

Title Page

Abstract

Introduction

Conclusions

References

Tables

Figures

◀

▶

◀

▶

Back

Close

Full Screen / Esc

Printer-friendly Version

Interactive Discussion



19, 3903–3931, 2006.

Schulz, C., Koch, J. D., Davidson, D. F., Jeffries, J. B., and Hanson, R. K.: Ultraviolet absorption spectra of shock-heated carbon dioxide and water between 900 and 3050 K, Chem. Phys. Lett., 355, 82–88, 2002.

5 Shemansky, D. E.: CO<sub>2</sub> Extinction Coefficient 1700–3000 Å, J. Chem. Phys., 56, 1582–1587, 1972.

Trinks, H. and Fricke, K. H.: Carbon dioxide concentrations in the lower thermosphere, J. Geophys. Res., 83, 3883–3886, 1978.

10 Yoshino, K., Esmond, J. R., Sun, Y., Parkinson, W. H., Ito, K., and Matsui, T.: Absorption cross section measurements of carbon dioxide in the wavelength region 118.7–175.5 nm and the temperature dependence. J. Quant. Spectrosc. Radiat. Transfer, 55, 53–60, 1991.

Zaragoza, G., López-Puertas, M., López-Valverde, M. A., and Taylor, F. W.: Global distribution of CO<sub>2</sub> in the upper mesosphere as derived from UARS/ISAMS measurements, J. Geophys. Res., 105, 19829–19839, 2000.

15

ACPD

9, 11551–11587, 2009

---

## Observations and analysis using the extended CMAM

S. R. Beagley et al.

---

Title Page

Abstract

Introduction

Conclusions

References

Tables

Figures

◀

▶

◀

▶

Back

Close

Full Screen / Esc

Printer-friendly Version

Interactive Discussion



**Observations and  
analysis using the  
extended CMAM**

S. R. Beagley et al.

**Table 1.** Scenarios analysed.

Scenario	Details
A-control	$K_{ZZ}$ (GWD) included, standard rate constants and J values
B	J(CO <sub>2</sub> ) increased by a factor of 5 otherwise A
C	$K_{ZZ}$ (GWD)=0, otherwise A
D	B+C
E	CO+OH reduced by factor of 5, otherwise A
F	Molecular diffusion for CO <sub>2</sub> set to zero, otherwise A

[Title Page](#)[Abstract](#)[Introduction](#)[Conclusions](#)[References](#)[Tables](#)[Figures](#)[I◀](#)[▶I](#)[◀](#)[▶](#)[Back](#)[Close](#)[Full Screen / Esc](#)[Printer-friendly Version](#)[Interactive Discussion](#)

Observations and  
analysis using the  
extended CMAM

S. R. Beagley et al.

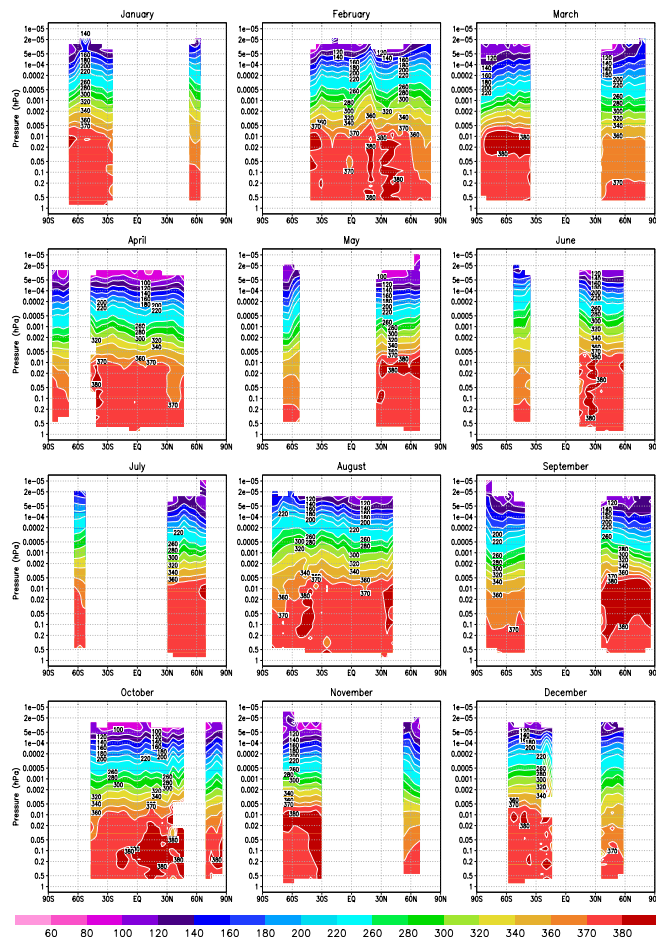


**Fig. 1.** Zonally and monthly averaged ACE CO<sub>2</sub> data (sunrise and sunset) for the period 21 February 2004 to 30 August 2007 versus latitude and pressure. The units are ppmv for the CO<sub>2</sub> mixing ratio.

Title Page

Abstract

Introduction

Conclusions

References

Tables

Figures

◀

▶

◀

▶

Back

Close

Full Screen / Esc

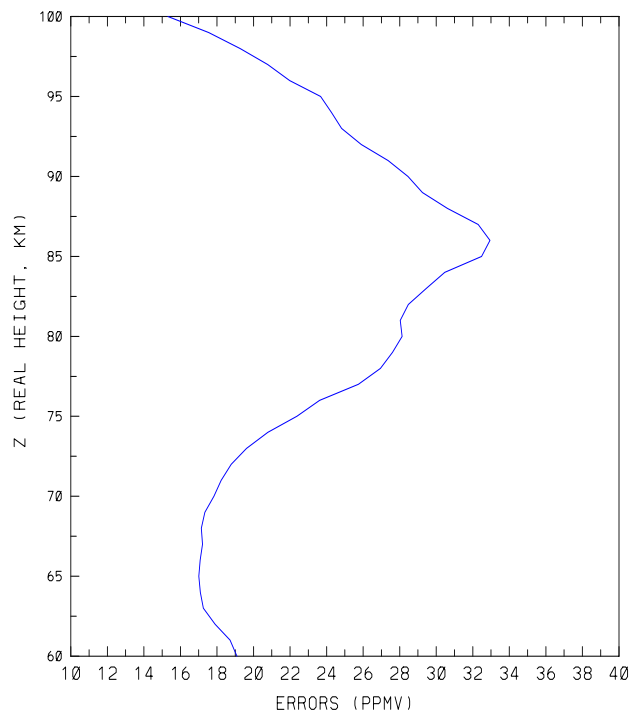
Printer-friendly Version

Interactive Discussion



**Observations and  
analysis using the  
extended CMAM**

S. R. Beagley et al.

**Fig. 2.** Global estimate of ACE uncertainties in CO<sub>2</sub> mixing ratio with height.[Title Page](#)[Abstract](#)[Introduction](#)[Conclusions](#)[References](#)[Tables](#)[Figures](#)[◀](#)[▶](#)[◀](#)[▶](#)[Back](#)[Close](#)[Full Screen / Esc](#)[Printer-friendly Version](#)[Interactive Discussion](#)

**Observations and analysis using the extended CMAM**

S. R. Beagley et al.

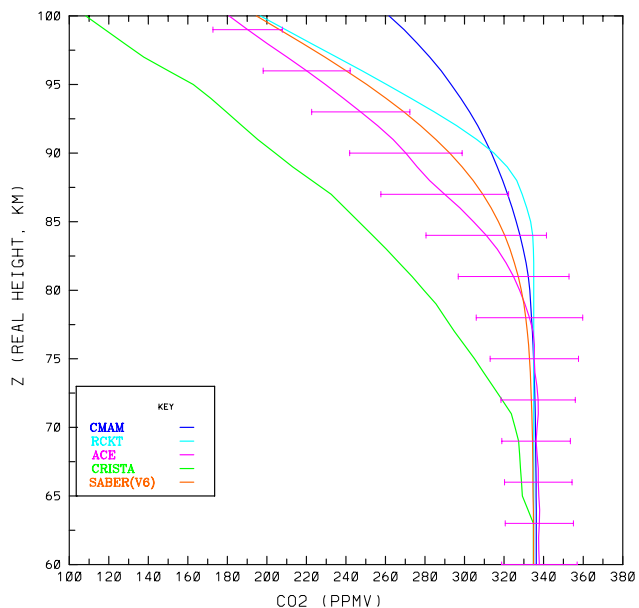


**Fig. 3.** A comparison of mean rocket measurements (compilation by Fomichev et al., 1998), global mean CRISTA observations (Kaufmann et al., 2002), daytime V1.06 SABER observations (see text for details), global mean ACE measurements and global mean CMAM CO<sub>2</sub>. Error bars indicate the CO<sub>2</sub> uncertainties in ACE measurements.

[Title Page](#)[Abstract](#)[Introduction](#)[Conclusions](#)[References](#)[Tables](#)[Figures](#)[◀](#)[▶](#)[◀](#)[▶](#)[Back](#)[Close](#)[Full Screen / Esc](#)[Printer-friendly Version](#)[Interactive Discussion](#)

## Observations and analysis using the extended CMAM

S. R. Beagley et al.

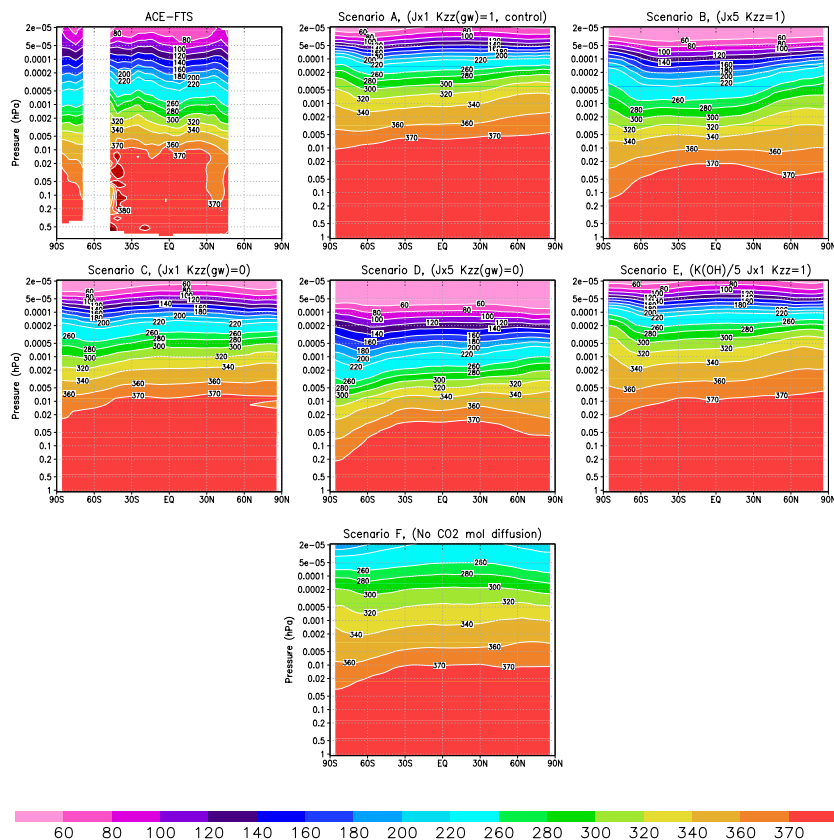


**Fig. 4.** Zonally and monthly averaged latitude-pressure plots of  $\text{CO}_2$  volume mixing ratios (ppmv) for April for the different scenarios shown in Table 1 used for the CMAM model and the ACE data (details same as Fig. 1).

Title Page

Abstract

Introduction

Conclusions

References

Tables

Figures

◀

▶

◀

▶

Back

Close

Full Screen / Esc

Printer-friendly Version

Interactive Discussion



## Observations and analysis using the extended CMAM

S. R. Beagley et al.

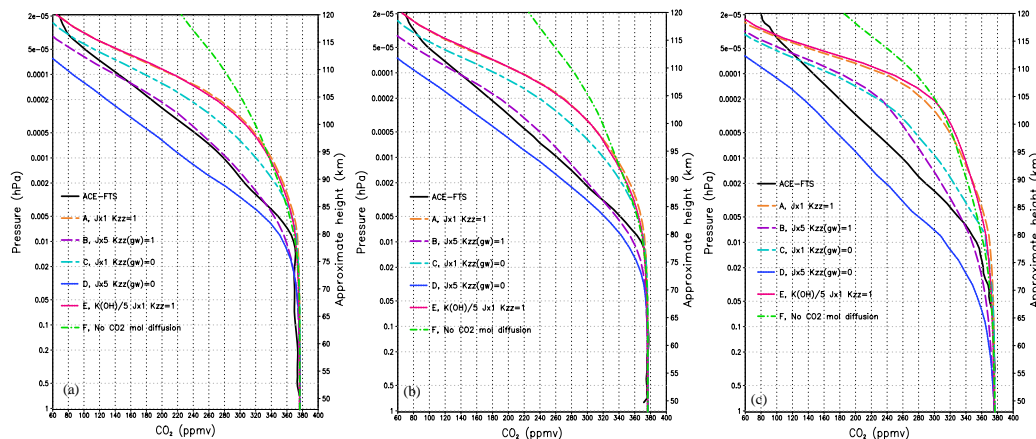


**Fig. 5.** ACE  $\text{CO}_2$  profiles from Figure 4, for latitudes **(a)**  $30^\circ$  N, **(b)**  $3^\circ$  N **(c)**  $80^\circ$  S. Also shown are the CMAM  $\text{CO}_2$  profiles for the various scenarios in Table 1.

Title Page

Abstract

Introduction

Conclusions

References

Tables

Figures

◀

▶

◀

▶

Back

Close

Full Screen / Esc

Printer-friendly Version

Interactive Discussion



**Observations and  
analysis using the  
extended CMAM**

S. R. Beagley et al.

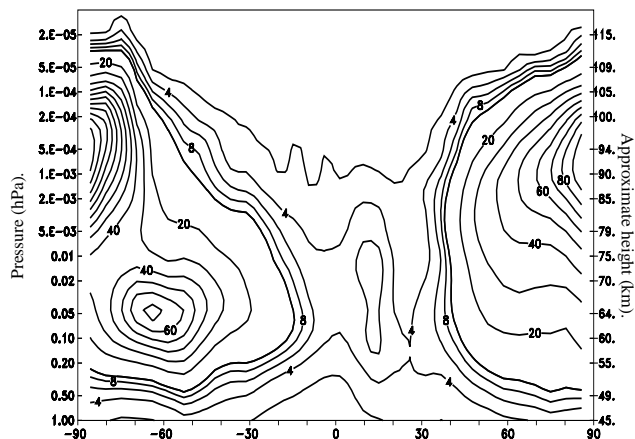


**Fig. 6.** Latitudinal-pressure plot of  $K_{ZZ}$  (GWD) in  $\text{m}^2/\text{s}$  for April from CMAM. Contour interval of 2 used in tropics and 10 in mid-high latitudes.

[Title Page](#)[Abstract](#)[Introduction](#)[Conclusions](#)[References](#)[Tables](#)[Figures](#)[◀](#)[▶](#)[◀](#)[▶](#)[Back](#)[Close](#)[Full Screen / Esc](#)[Printer-friendly Version](#)[Interactive Discussion](#)

Observations and  
analysis using the  
extended CMAM

S. R. Beagley et al.

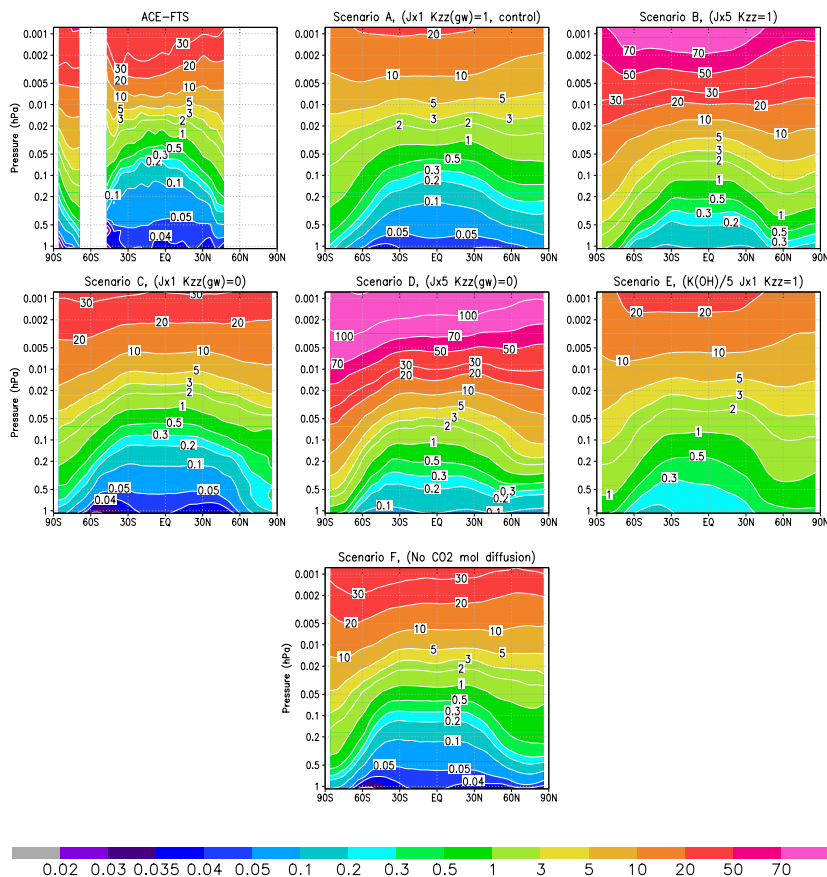


**Fig. 7.** Zonally and monthly averaged latitude-pressure plots of CO volume mixing ratios (ppmv) for April for the different scenarios shown in Table 1 used for the CMAM model and the ACE data (details same as Fig. 1).

Title Page

Abstract

Introduction

Conclusions

References

Tables

Figures

◀

▶

◀

▶

Back

Close

Full Screen / Esc

Printer-friendly Version

Interactive Discussion



## Observations and analysis using the extended CMAM

S. R. Beagley et al.

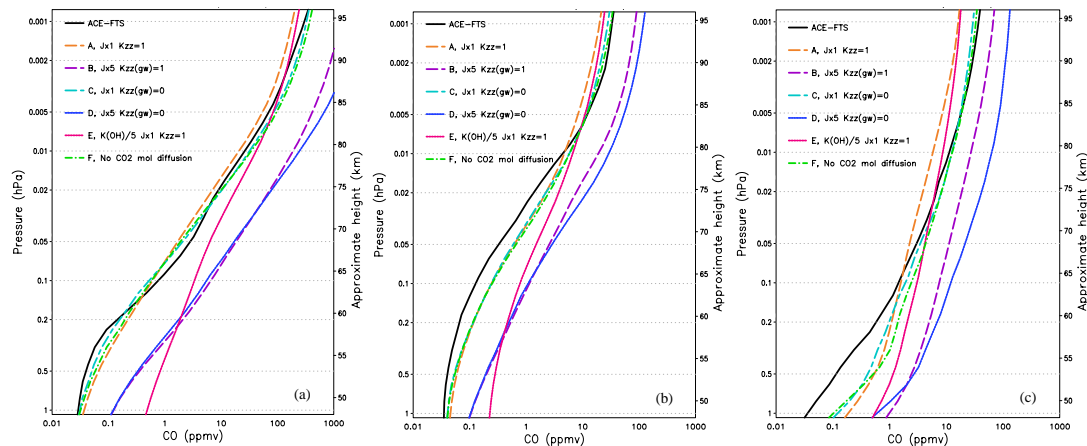


**Fig. 8.** ACE CO profiles from Fig. 7 for latitudes **(a)** 30° N, **(b)** 3° N **(c)** 80° S. Also shown are the CMAM CO profiles for the various scenarios in Table 1.

Title Page

Abstract

Introduction

Conclusions

References

Tables

Figures

◀

▶

◀

▶

Back

Close

Full Screen / Esc

Printer-friendly Version

Interactive Discussion



## Observations and analysis using the extended CMAM

S. R. Beagley et al.

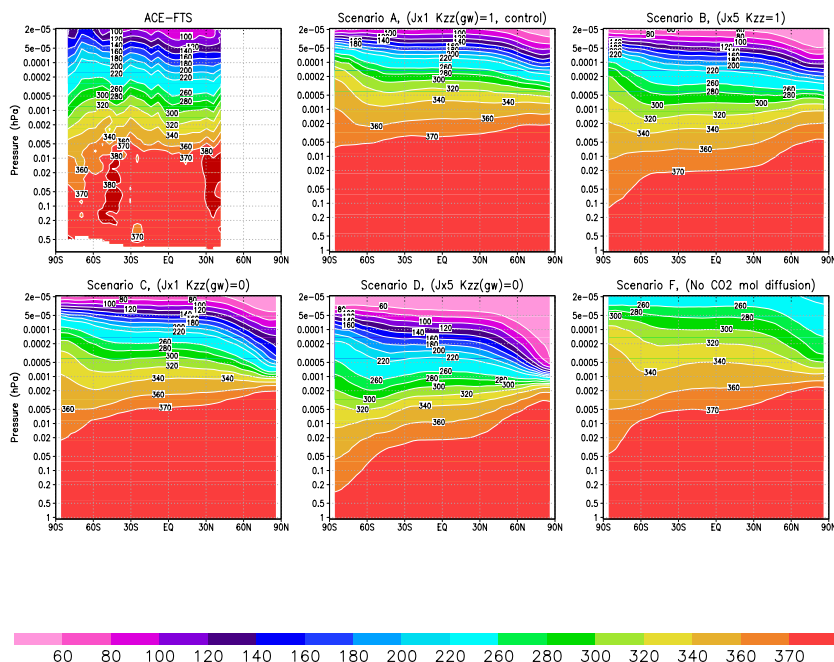


**Fig. 9.** Zonally and monthly averaged latitude-pressure plots of CO<sub>2</sub> volume mixing ratios (ppmv) for August for the different scenarios shown in Table 1 used for the CMAM model and the ACE data (details same as Fig. 1).

Title Page

Abstract

Introduction

Conclusions

References

Tables

Figures

◀

▶

◀

▶

Back

Close

Full Screen / Esc

Printer-friendly Version

Interactive Discussion



## Observations and analysis using the extended CMAM

S. R. Beagley et al.

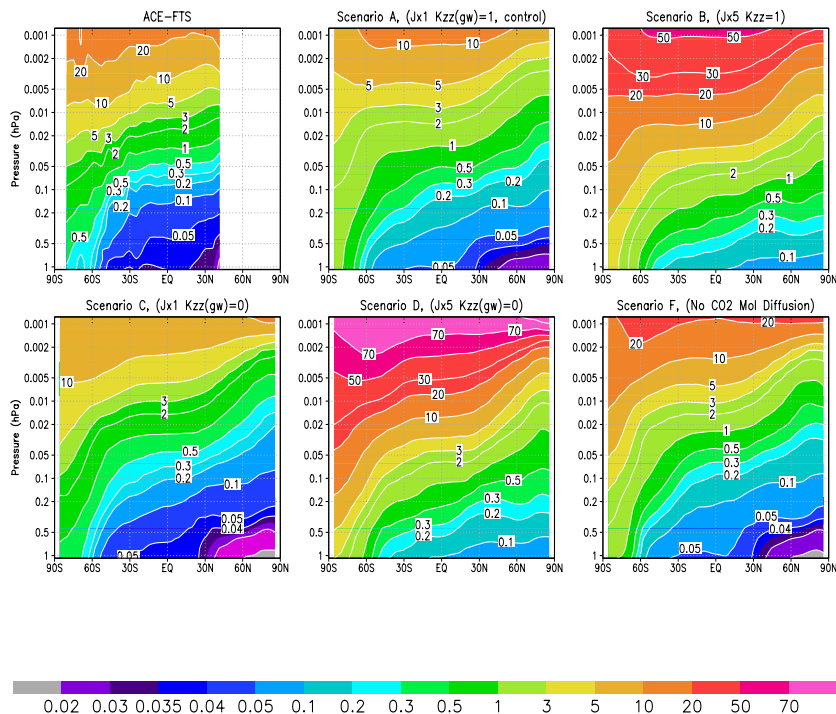


**Fig. 10.** Zonally and monthly averaged latitude-pressure plots of CO volume mixing ratios (ppmv) for August for the different scenarios shown in Table 1 used for the CMAM model and the ACE data (details same as Fig. 1).

Title Page

Abstract

Introduction

Conclusions

References

Tables

Figures

◀

▶

◀

▶

Back

Close

Full Screen / Esc

Printer-friendly Version

Interactive Discussion



Observations and  
analysis using the  
extended CMAM

S. R. Beagley et al.

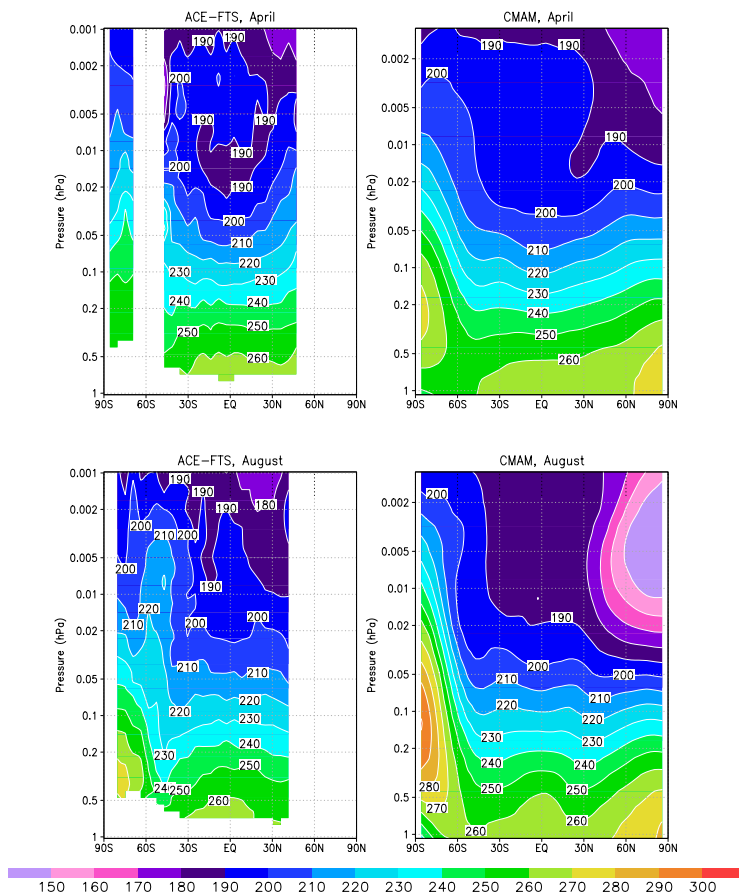


**Fig. 11.** Zonally and monthly averaged latitude-pressure plots of temperature (K) for the ACE data and for the control run (scenario A) for the CMAM model for April (top panels) and August (bottom panels).

[Title Page](#)[Abstract](#)[Introduction](#)[Conclusions](#)[References](#)[Tables](#)[Figures](#)[◀](#)[▶](#)[◀](#)[▶](#)[Back](#)[Close](#)[Full Screen / Esc](#)[Printer-friendly Version](#)[Interactive Discussion](#)